# GenPro4 Optical Model for Solar Cell Simulation and Its Application to Multijunction Solar Cells

Santbergen, Rudi; Meguro, Tomomi; Suezaki, Takashi; Koizumi, Gensuke; Yamamoto, Kenji; Zeman, Miro

**DOI**
10.1109/JPHOTOV.2017.2669640

**Publication date**
2017

**Document Version**
Accepted author manuscript

**Published in**
IEEE Journal of Photovoltaics

# GenPro4 Optical Model for Solar Cell Simulation and its Application to Multi-Junction Solar Cells

Rudi Santbergen, Tomomi Meguro, Takashi Suezaki, Gensuke Koizumi, Kenji Yamamoto and Miro Zeman

***Abstract*— We present a new version of our optical model for solar cell simulation: GENPRO4. Its working principles are briefly explained. The model is suitable for quickly and accurately simulating a wide range of wafer based and thin-film solar cells. Especially adjusting layer thicknesses to match the currents in multi-junction devices can be done with a minimum of computational cost. To illustrate this, a triple junction thin-film silicon solar cell is simulated. The simulation results show very good agreement with EQE measurements. The application of an $MgF_2$ anti-reflective coating or an anti-reflective foil with pyramid texture is considered. Their effects on the implied photocurrents of top, middle and bottom cell are investigated in detail.**

***Index Terms*—Modeling, Thin Film PV Device Properties and Modeling, Geometrical Optics.**

## I. INTRODUCTION

Solar cells are complex optical devices, employing advanced light incoupling and trapping strategies. Optical simulations are an important tool for solar cell design and provide detailed insight in reflection and parasitic absorption losses. These simulations require an optical model that, for a given solar cell structure, calculates the reflectance, absorptance and transmittance as a function of wavelength, taking into account scattering of light at the interfaces and trapping of light inside of the solar cell. In case the optical model is coupled to an *electrical* model for calculation of the solar cell's current-voltage characteristics, the optical model also needs to provide the photon absorption profile along the depth of the absorber layer [1-5].

Most of the existing optical models are either based on wave optics or ray optics. Wave optics models take the full electromagnetic wave nature of light into account by rigorously solving the Maxwell equations. Due to the high computational cost these Maxwell solvers are limited to small simulation domains, so only periodic thin-film solar cells can be simulated within reasonable computation time [6]. Ray optics on the other hand approximates light as rays. Ray tracing techniques are commonly used to simulate textured c-Si solar cells [7,8]. However, because wave effects like diffraction are ignored, ray optics is not suitable for simulating light scattering by sub-wavelength features.

In most commercially available Maxwell solvers or ray tracing software it is possible to create a 3D model of a complete solar cell. However, in many cases the solar cell can, to a good approximation, be represented as a 1D multilayer structure. This allows the use of simpler and faster multilayer methods. In case all interfaces are optically flat, straightforward transfer-matrix or net-radiation methods can be used [9,10]. In case the interfaces have a texture that scatters light, extended multilayer methods can be used [11-16]. We previously introduced the extended net-radiation method [17,18] and similar methods have been proposed since [19,20]. The extended net-radiation method takes the angular intensity distribution of scattered light for every interface as input. A simple intensity distribution (e.g. Lambertian) can be assumed or a more realistic distribution can be calculated taking into account the dependence on wavelength and the angle of incidence by using dedicated interface models. In our previous implementation a Phong distribution [21] was assumed for sub-wavelength textured interfaces and a 2D ray tracing model was used for interfaces with larger textures.

In this paper we introduce a new, much improved version of our optical model for solar cell simulation: GENPRO4. The novelty is not so much the use of the extended net-radiation method, which we [17,18] and others [19,20] have presented before, but the addition of fast and flexible interface models for light scattering at textured interfaces. Interfaces with sub-wavelength random texture are simulated using the scalar scattering model developed by Jäger et al. [22,23]. Interfaces with larger texture are simulated using ray tracing. Both interface models are fully 3D and can take an atomic force microscopy (AFM) scan of the surface morphology as input. Angular intensity distributions calculated by commercially available Maxwell solvers, as done by Li et al. [19], can be given as input as well. In addition we include new algorithms for detailed analysis of reflection losses and for current matching in multi-junction solar cells. GENPRO4 has been validated for a wide range of wafer based and thin-film solar

Manuscript received mm-dd-yyyy; accepted received mm-dd-yyyy. Date of publication received mm-dd-yyyy; date of current version received mm-dd-yyyy.

R. Santbergen and M. Zeman are with Delft University of Technology, 2628CD Delft, the Netherlands. T. Meguro T. Suezaki, G. Koizumi and K. Yamamoto are with Kaneka Corporation, Osaka 566-0072, Japan.(e-mail: r.santbergen@tudelft.nl).

cells [24-26] and is now commercially available to the solar cell community [27].

In section II the working principles of GENPRO4 are explained. Then in section III we illustrate its new features by considering a triple junction thin-film silicon solar cell. We analyze the effects of an $MgF_2$ anti-reflection coating and an anti-reflective foil with pyramid texture on the implied photocurrents of top, middle and bottom cell. Finally, in section IV the conclusions are presented.

## II. MODEL DESCRIPTION

This section explains the extended net-radiation method on which GENPRO4 is based. More details can be found in the GENPRO4 user manual [28]. The method is completely general and can be applied to both wafer based and thin-film solar cells.

### A. Flat interfaces

In the simplest case where all interfaces are flat, the conventional net-radiation method can be used [10]. In the net-radiation method the solar cell is represented as a multilayer structure as shown in Fig. 1. We number the layers and interfaces from top to bottom. The subscript $i$ will be used to indicate layer and interface numbers. The goal of the simulation is to determine the overall reflectance $R$, the transmittance $T$ and the absorptance of each layer $A_i$. Each layer is characterized by thickness $d_i$ and complex refractive index $N_i(\lambda)$, where $\lambda$ is the wavelength. Because $N_i$ is wavelength dependent, $R$, $T$ and $A_i$ are wavelength dependent as well. Below it is explained how $R$, $T$ and $A_i$ are calculated for a single wavelength. This calculation is then repeated for every wavelength in the relevant wavelength range.

When all interfaces are optically flat, the interface reflectances $r_i$ can be calculated from the Fresnel equation and the corresponding interface transmittances are given by $t_i = 1-r_i$. The *layer* transmittances $\tau_i$ can be calculated from the Lambert-Beer law. Note that the values of $r_i$, $t_i$ and $\tau_i$ depend on the angle of incidence. An incident photon can bounce between the interfaces multiple times and travel a complicated path (see Fig. 1a). Therefore, to calculate $R$, $T$ and $A_i$ from $r_i$, $t_i$ and $\tau_i$, all possible reflections have to be taken into account. There are different mathematically equivalent methods to do this. The net-radiation method, is illustrated in Fig. 1b. At every interface four fluxes are defined: $q_i^x$. Here subscript $i$ is the interface number and the superscript $x$ ( = $a$, $b$, $c$ or $d$) indicates whether the light is approaching/leaving the interface from the top/bottom, as defined in Fig. 1b. Each flux represents the net-radiation (in W/m$^2$) due to all possible photon paths. All fluxes are related by a set of linear equations [10]:

$$\begin{cases} q_i^a = \tau_i \cdot q_{i-1}^d \\ q_i^b = r_i \cdot q_i^a + t_i \cdot q_i^c \\ q_i^c = \tau_{i+1} \cdot q_{i+1}^b \\ q_i^d = t_i \cdot q_i^a + r_i \cdot q_i^c \end{cases} \quad (1)$$

In total there are $4 \cdot I$ equations, where $I$ is the total number of interfaces. It is convenient to normalize all fluxes to the incident power, such that they can be written in non-dimensional form. The assumption that all light is incident from the top and none from the bottom then implies that $q_1^a = 1$ and $q_I^c = 0$. Eq. (1) represents a set of linear equations that can be solved using standard numerical techniques to obtain the values of every flux. From this, the desired $R$, $T$ and $A_i$ are obtained

$$R = q_1^b \quad (2)$$

$$T = q_I^d \quad (3)$$

$$A_i = q_{i-1}^d - q_{i-1}^c + q_i^b - q_i^a \quad (4)$$

Note that $A_i$ is simply the sum of fluxes entering minus the fluxes leaving layer $i$.

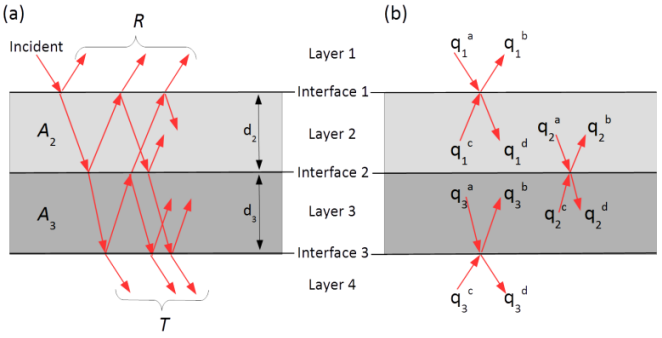


Fig. 1. Schematic representation of a multilayer structure showing the numbering convention for layers and interfaces. a) Various optical paths contributing to $R$, $T$ and $A_i$. b) Net-radiation fluxes.

### B. Interference

The fluxes $q$ introduced in section IIA represent the light intensities in W/m$^2$. In eq. (1) and (4) these fluxes are simply being added without taking into account interference effects. This approach is only accurate for so-called incoherent layers that are thick compared to the coherence length of the incident sunlight (≈ 1 μm). For thin (coherent) layers, interference does play a role and GENPRO4 uses a different calculation method in which the fluxes represent the complex amplitudes of electromagnetic waves [11]. GENPRO4 can combine these two distinct approaches by treating the thin (coherent) layers as a 'coating', which is part of the interface between two thick (incoherent) 'layers'. In GENPRO4 'layers' are treated incoherently and do not give rise to interference while 'coatings' are treated coherently and do give rise to interference. Note that GENPRO4 calculates the photon absorption profile of both the coherent and incoherent layers using the method described in ref. 11.

### C. Surface Texture

Most interfaces in the solar cell have a surface texture to reduce reflection losses and to scatter incident light into the absorber layer. In that case, instead of having one discrete propagation direction, the reflected and transmitted light is characterized by an angular intensity *distribution* over the available propagation directions. Each propagation direction

can be visualized as a point on a hemisphere, characterized by zenith angle $\theta$ and azimuth angle $\varphi$. The net-radiation method described in section IIA can then be extended by sub-dividing this hemisphere into angular intervals each with a corresponding sub-flux. In this case we use a discretization scheme that divides the hemisphere into cones, such that each of the angular intervals is bounded by an upper and lower zenith angle $\theta$, as indicated in Fig. 2a. The zenith angle is measured relative to the surface normal direction and ranges from 0° (perpendicular to the interface) to 90° (parallel to the interface). Typically the number of angular intervals is set to 30, resulting in an angular width of the intervals of 3°. Each flux is then divided into 30 sub-fluxes as indicated in Fig. 2b. All relations between these sub-fluxes can still be written as a set of linear equations. Note that this set now contains $4 \cdot I \cdot V$ equations, where $I$ and $V$ are the number of interfaces and the number of angular intervals, respectively. Typically this results in a large set of hundreds of equations. However, using standard numerical techniques a computer can solve such a set of linear equations within a fraction of a second.

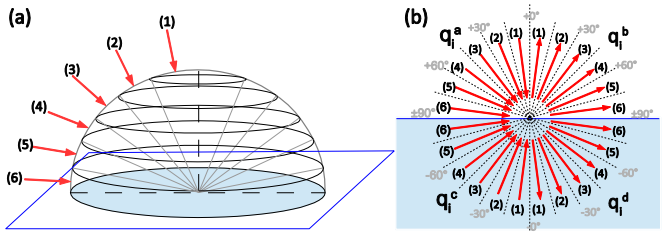


Fig. 2. a) Division of every hemispherical direction into angular intervals. b)Net-radiation sub-fluxes at interface 1. (For clarity the figure shows six intervals. GENPRO4 typically uses 30 intervals for higher accuracy.)

It is convenient to indicate each sub-flux in the following way: $q_i^x(v)$, where $x$ and $i$ have the same meaning as explained in section IIA, and $v$ is the interval number. For example $q_2^a(5)$ is the flux approaching interface 2 from above in the 5th angular interval (i.e. the interval ranging from 12° to 15°). The fluxes can then be grouped into vectors $\boldsymbol{q}_i^x = [q_i^x(1),\ q_i^x(v), \ldots, q_i^x(V)]$, where the bold font indicates a vector. $V$ is the number of intervals, which typically is 30. This vector notation allows the large set of equations to be written in a compact way using matrix multiplication

$$\begin{cases} \boldsymbol{q}_i^a = \boldsymbol{\tau}_i \cdot \boldsymbol{q}_{i-1}^d \\ \boldsymbol{q}_i^b = \boldsymbol{r}_i^+ \cdot \boldsymbol{q}_i^a + \boldsymbol{t}_i^- \cdot \boldsymbol{q}_i^c \\ \boldsymbol{q}_i^c = \boldsymbol{\tau}_{i+1} \cdot \boldsymbol{q}_{i+1}^b \\ \boldsymbol{q}_i^d = \boldsymbol{t}_i^+ \cdot \boldsymbol{q}_i^a + \boldsymbol{r}_i^- \cdot \boldsymbol{q}_i^c \end{cases} \quad (5)$$

Note that the coefficients $\boldsymbol{r}_i$, $\boldsymbol{t}_i$ and $\boldsymbol{\tau}_i$ are now also in bold to indicate that these are now matrices of size $V \times V$. The matrices $\boldsymbol{r}_i$ and $\boldsymbol{t}_i$, to which we will refer as scattering matrices, contain the angular intensity distribution of scattered light for every angle of incidence (also known as the bi-directional scatter distribution function). The $\boldsymbol{r}_i$ and $\boldsymbol{t}_i$ matrices for light incident on interface $i$ from the top and bottom are different and the superscripts '+' and '-' are used to distinguish them. The scattering matrices are calculated from the surface morphology of the interface using either the ray optics model or the wave optics model, as will be illustrated in section IID. Once the matrices are calculated, they can be substituted into eq. (5) and the set of equations can be solved.

The vector $q_1^b$ contains all fluxes leaving the top of the first interface (see Fig. 2b) and therefore contains the information regarding the angular intensity distribution of light reflected by the multilayer structure. The total reflectance $R$ is simply sum of the intensity of all the elements of this vector $\sum \boldsymbol{q}_1^b = q_1^b(1) + q_1^b(2) + \cdots + q_1^b(V)$. Similar to eq. (2-4), $R$, $T$ and $A_i$ are given by

$$R = \sum \boldsymbol{q}_1^b \quad (6)$$

$$T = \sum \boldsymbol{q}_I^d \quad (7)$$

$$A_i = \sum \boldsymbol{q}_i^d - \sum \boldsymbol{q}_i^c + \sum \boldsymbol{q}_{i+i}^b - \sum \boldsymbol{q}_{i+1}^a \quad (8)$$

### D. *Calculation of Scattering Matrices*

As explained above, every interface $i$ is characterized by four scattering matrices $(\boldsymbol{r}_i^+, \boldsymbol{t}_i^+, \boldsymbol{r}_i^-, \boldsymbol{t}_i^-)$. Matrix element $(u,v)$ indicates the probability that a photon, incident from angular interval $v$, after reflection or transmission ends up in interval $u$. For visualization purposes we place these scattering matrices in a 2 × 2 array to form one single matrix as shown in Fig. 3. The horizontal axis of the matrix represents the incident angle and the vertical axis represents the outgoing angle. As also indicated in Fig. 2b, these angles go from +0° (normal incidence from above the interface) to ±90° (parallel to the interface) and back to -0° (normal incidence from below

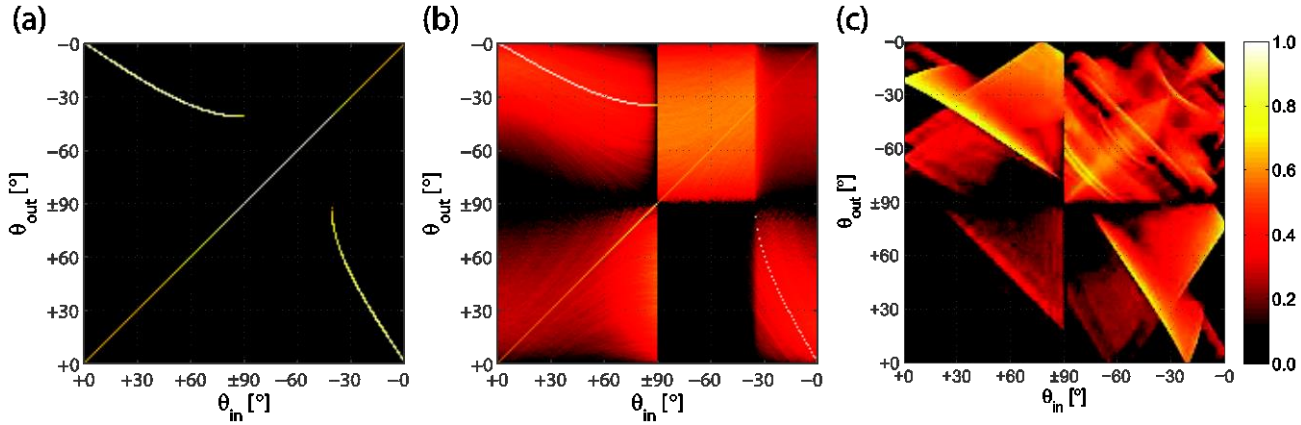


Fig. 3. Scattering matrices calculated by GENPRO4 for a) a flat air/glass interface. b) an interface with Asahi U-type texture (calculated for λ = 600 nm). c) an air/glass interface with an inverted pyramid texture with a steepness of 55°.

the interface). Plus and minus signs are used to indicate whether an angle is measured from the surface normal above or below the interface. The color indicates the corresponding probability which ranges from 0% (black) to 100% (white). Each quadrant of the matrices shown in Fig. 3 consists of one scattering matrix with 90 × 90 elements, corresponding to a small angular interval of 1°. The number of intervals can be increased to improve accuracy at the cost of increased simulation time. Intervals of 3°, resulting in scatter matrices of 30 × 30 elements, usually provide a good trade-off between accuracy and simulation time. Note that conservation of energy dictates that the sum of every column adds up to 100%. The reciprocity theorem [29] dictates that if light can go from interval *u* to *v*, the reverse path *v* to *u* should also be allowed, which implies that the matrix should be symmetrical.

*Model for Flat Interfaces*

A basic ray-optics model based on the Fresnel equations for reflectance and Snell's law for refraction angles is used for flat interfaces. Here we consider a flat air/glass interface of which the resulting scattering matrices are shown in Fig. 3a. The line on the main diagonal represents the specular reflection component, because for specular reflection a photon incident in interval *u* is reflected back into the same interval *u*. The other lines (near the counter diagonal) represent the transmission component. As a result of refraction these lines are curved and terminate at the critical angle. The sum of each column adds up to 100% indicating that energy is conserved. Also the matrix is symmetrical, which is in agreement with the reciprocity theorem.

*Model for Interfaces with Small Texture*

For surface textures with features smaller than the wavelength, wave effects like interference and diffraction need to be taken into account. For this the scalar scattering model developed by Jäger et al. [22,23] was implemented in GENPRO4. Input for this model is a height map of the surface morphology. The interface is then approximated by an array of point sources, each emitting spherical scalar waves at a phase calculated from the local height of the morphology and the angle of incidence. The scattering intensity for a particular direction depends on whether these waves interfere constructively or destructively in the far field. Mathematically this is equivalent to taking the Fourier transform of the pupil function. This scalar scattering model has been experimentally validated for a wide range of surface morphologies and was shown to be most accurate for morphologies with feature sizes on the order of 100 nm or less [22,23].

Amorphous silicon (a-Si:H) solar cells are commonly deposited onto an Asahi U-type glass/SnO:F substrate. This has a surface texture with a root mean square roughness of about 50 nm. Its morphology was measured using AFM and used as input for the scalar scattering model. Fig. 3b shows the corresponding scattering matrices calculated for an SnO:F/a-Si:H interface with this texture. The diffusely reflected and transmitted light is scattered over a broad angular range, distributing the probabilities over a wide range of intervals. The *specular* reflection and transmission components are visible as the thin lines. The sum of each column again adds up to 100% indicating that energy is conserved. However, Fig. 3b reveals that the matrix is not symmetrical, which means that the scalar scattering model developed by Jäger et al. is not reciprocal. This limitation, which we have exposed by displaying the scatter matrices in this way, means that care should be taken when using this model. In section III we will however, show by means of experimental validation that the model is accurate for the thin-film silicon solar cell considered.

*Model for Interfaces with Large Texture*

For surface textures with a feature size that is large compared to the wavelength, wave effects can be ignored and ray optics applies. For this, GENPRO4 uses a built-in ray tracing model. To calculate column *u* of the interface matrix, incident rays are emitted onto the textured interface from interval *u* and the angular intensity distribution of rays reflected and transmitted by the interface is recorded. This is then repeated for every incident angular interval. Fig. 3c shows the resulting scattering matrices of an air/glass interface with an inverted pyramid texture with a steepness of 55°. This figure shows that for a given angle of incidence, a ray can be reflected or transmitted in various directions. This is because each pyramid has four facets, each with a different orientation, that can be hit by the ray one or multiple times. The sum of each column adds up to 100% indicating that energy is conserved. Also the matrix is symmetrical, from which it can be concluded that the ray tracing model does not violate the reciprocity theorem.

*External Models*

The three interface models mentioned above are included in GENPRO4. With these models most types of c-Si and thin-film solar cells can be simulated accurately. However, some effects, such as plasmonic effects and refractive index grading, are not included. These effects can nonetheless be simulated for a single interface using external models such as a Maxwell solver or an effective medium model. As long as the external model can predict the angular intensity distribution of reflected and transmitted light as a function of the angle of incidence, this information can be imported by GENPRO4 in the form of a scattering matrix and included in the simulation. In this way different simulation techniques, each optimized for a particular interface, can be combined in a computationally efficient way. By displaying the generated scattering matrices as shown in Fig. 3, one can quickly check whether conservation of energy and reciprocity are obeyed.

### *E. Features of the Model*

The extended net-radiation method is very fast and efficient and a typical simulation takes only a few minutes. In GENPRO4 most computation time is spent on calculating the scattering matrices $\boldsymbol{r}_i$ and $\boldsymbol{t}_i$ for every wavelength. When repeating the simulation with a different layer thickness, the corresponding layer transmittance matrix $\boldsymbol{\tau}_i$ changes, but the scattering matrices $\boldsymbol{r}_i$ and $\boldsymbol{t}_i$ stay the same. In that case the previously calculated scattering matrices can be re-used without recalculation to save computation time. This is especially useful for matching the currents between sub-cells

of a multi-junction solar cells by varying absorber layer thicknesses, as will be illustrated in the next section.

In the next section we simulate multi-junction solar cells under normally incident light. In that case the incident flux is in the first angular interval of $\boldsymbol{q}_1^a$. However, it is also possible to have this flux incident in any other angular interval of $\boldsymbol{q}_1^a$ and simulate the cell under a different angle of incidence. One could even distribute the incident flux over several intervals to mimic the angular distribution of diffuse light coming from different parts of the sky.

The simplifying assumptions that make the GENPRO4 model fast, also give rise to some limitations that have to be considered. Firstly, the model represents the solar cell as a multilayer system. 3D structures that deviate from this, like metal contact fingers, cannot be included in the simulation. Also the calculated photon absorption profile along the depth of the absorber layer is a 1D cross-section. 3D non-uniformities are not resolved. Secondly, for this work we have not discretized the angular intervals with respect to the azimuth angle (see Fig. 2a). This is convenient for flat interfaces or random textures with rotation symmetry around the surface normal, but it is less accurate for periodic textures that do not have this rotation symmetry, such as gratings or grooves.

## III. RESULTS

In this section we consider the triple junction thin-film silicon solar cell design by Kaneka Corporation, indicated in Fig 4a. The top, middle and bottom cell are amorphous silicon (a-Si:H), amorphous silicon/germanium alloy (a-SiGe:H) and nano-crystalline silicon (nc-Si:H). The bandgaps of these respective materials are 1.8 eV, 1.5 eV and 1.1 eV. Each cell consists of an intrinsic absorber layer with 10 to 20 nm thin p and n-type regions at the front and rear, respectively. Two low-index intermediate reflector layers separate the top and middle cell and the middle and bottom cell, respectively [29]. The whole layer stack was deposited onto a glass/$SnO_2$:F superstrate (Asahi U-type). The $SnO_2$:F is approximately 700 nm thick and serves as transparent front contact. In addition it has a surface texture with an rms roughness of about 50 nm, to scatter the incident light. At the rear side there is a back reflector consisting of 100 nm of ZnO:Al and 300 nm of silver.

In this initial design, the thicknesses of top, middle and bottom intrinsic layer (i-layer) are 100.0 nm, 112.5 nm and 2300 nm, respectively. This triple junction device was fabricated by Kaneka Corporation. The external quantum efficiencies (EQE) of top, middle and bottom cell were measured and the result is shown in Fig. 4b (symbols). This shows that the top, middle and bottom cell each absorb a different part of the spectrum. The corresponding short circuit current densities, obtained by integrating the EQE curves over the AM1.5g spectrum, are indicated as well. This shows that the bottom cell generates the lowest current density of 7.70 mA/cm$^2$ and therefore limits the current of the total device.

GENPRO4 was used to simulate the layer structure of Fig. 4a in the wavelength range 300 to 1200 nm in steps of 10 nm. The layer thicknesses mentioned above were used and the refractive index and extinction coefficient of each layer was measured in-house using spectral ellipsometry and/or reflection/transmission measurements. In principle such thin i-layers could give rise to interference fringes in the EQE curves. However, the measured EQE curves shown in Fig. 4b do not show such fringes. Most likely these interference fringes are suppressed by the strong light scattering due to the surface textures. For this reason we simulate the i-layers incoherently. The first two interfaces (air/glass and glass/$SnO_2$:F) are flat. The $SnO_2$:F superstrate has a nano-texture designed for light scattering and its surface morphology was measured using AFM over an area of 20 µm × 20 µm. All subsequent interfaces have a nano-texture as well. The most accurate simulation results are obtained when the measured morphology of every interface is used as input [22,23]. However, here we use the simplifying assumption that deposition is perfectly conformal, such that all subsequent interfaces have the same texture. To make sure that this assumption does not introduce a significant error, experimental validation will be presented below. The angular intensity distribution of light scattered by the textured interfaces was simulated using the scalar scattering model with the AFM scan of the surface morphology as input [22,23].

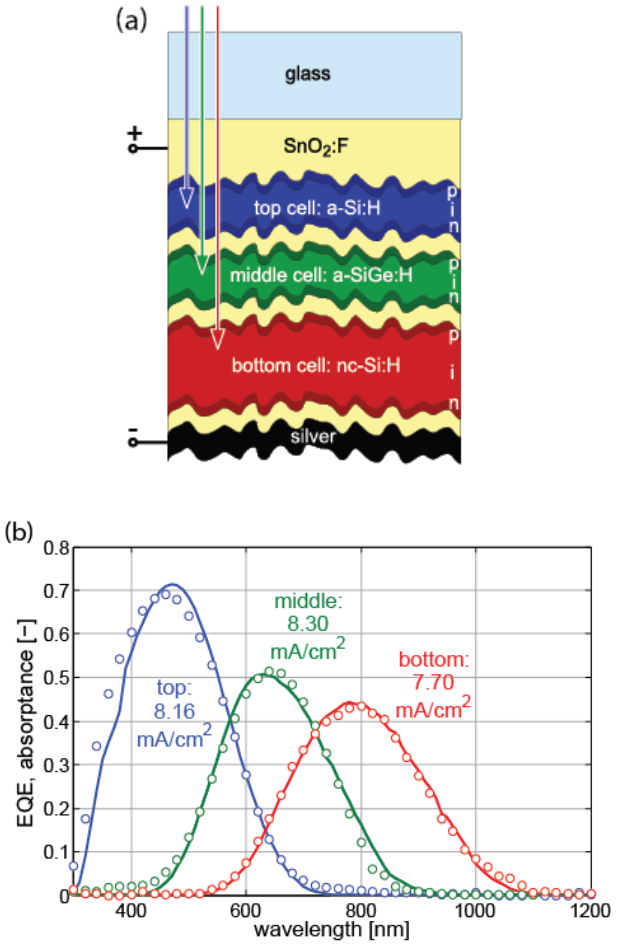


Fig. 4. a) Schematic cross-section of triple junction thin-film silicon solar cell. b) Measured EQE (circles) and simulated absorptance in i-layer (lines) of top, middle and bottom cells.

GENPRO4 gives the reflectance, absorptance of each layer and the transmittance as a function of wavelength. The absorptances of the top, middle and bottom i-layer, calculated for normal incidence, are shown in Fig. 4b (lines) and compared with the measured EQE (circles). For state-of-the-art devices it is accurate to assume that every photon absorbed in the i-layer generates one electron-hole pair and recombination losses can be ignored. In that case the absorptance of the i-layer should be identical to the cell's EQE. Fig. 4b shows that there is very good agreement between measurement and simulation. This simulation result shows that GENPRO4 is a valid tool for simulating this type of solar cell. In addition it shows that for this type of solar cell a purely optical simulation can be used to predict EQE curves and the corresponding short circuit current densities. Note that if losses due to recombination of photogenerated charge carriers play a more important role, an electrical model that takes these effects into account would have to be needed to accurately predict the EQE.

Next the simulation is repeated for different top and middle i-layer thicknesses while keeping the thickness of the bottom cell fixed at 2300 nm. In all simulations normal incidence is assumed and the current densities are obtained by integrating over the AM1.5g spectrum. The goal is to determine the thickness combination that results in perfectly matched cell currents. Because the scattering matrices calculated in the first simulation can be reused, each simulation finishes within a few seconds. This means that it is feasible to simulate many thickness combinations. We vary both top and middle i-layer thickness from 50 to 150 nm in steps of 5 nm. The result of more than 400 simulations is shown in Fig. 5a. It shows the *device* current density as a function of top and middle cell thickness for a fixed bottom cell thickness of 2300 nm. Note that this device current density is the *limiting* current, i.e. the lowest current generated by the top, middle or bottom cell. When the top cell is thin (region indicated in blue), it limits the device current. When the middle cell is thin (region indicated in green), this cell limits the device current. When both top and middle cell are thick (region indicated in red), the bottom cell limits the device current. The highest device current is obtained when all currents are perfectly matched. The simulation shows that this is the case when the top cell is 94.0 nm thick (instead of 100.0 nm) and the middle cell is 99.5 nm thick (instead of 112.5 nm). At this point the device current density is 7.98 mA/cm$^2$. Therefore, relative to the initial device considered in Fig. 4b, *decreasing* the thickness of top and middle i-layer *increases* the device current by 3.6%. Note that in practice it is difficult to deposit this films of this exact layer thickness with sub-nanometer accuracy uniformly and reproducibly over large areas. The mentioned thicknesses should therefore be interpreted as target thicknesses and the corresponding increase in device current as the theoretically maximum achievable current gain.

Fig. 5b shows the absorptance of each layer as a function of wavelength in the current matched device. The desired absorption in the i-layers is indicated by the light brown area and the contributions from top, middle and bottom i-layer are indicated by the blue, green and red lines. Integrating these curves over the AM1.5g spectrum confirms that top, middle and bottom cell generate exactly the same current density of 7.98 mA/cm$^2$. Besides the desired absorption, there are significant parasitic absorption losses as well. The yellow and orange area represent the absorption losses in $SnO_2$:F and the combined absorption losses in the p and n-layers. The white area represents the reflectance loss.

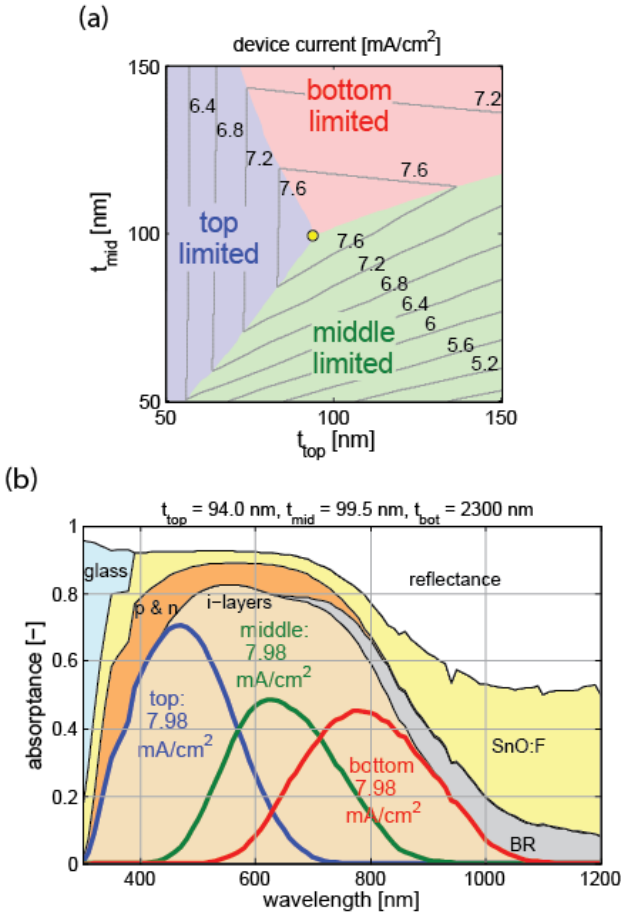


Fig. 5. a) Device current density (in mA/cm$^2$) as a function of top and middle i-layer thickness. Blue, green and red areas indicate where respectively top, middle or bottom cell are current limiting. The maximum current is obtained where all currents are matched (indicated by yellow circle). b) Absorptance of every layer and reflectance for the current matched triple junction cell.

The reflectance loss is one of the largest optical losses and two approaches for reflection reduction are tried. Firstly the effect of an $MgF_2$ anti-reflective coating, with a refractive index of about 1.38, is investigated. A bare air/glass interface has a constant reflectance of 4%. A $MgF_2$ coating reduces this to less than 2%, but only in the wavelength range near a reflection minimum. The first order reflection minimum occurs at a wavelength that is 4 times the coating's optical thickness. Therefore, with increasing coating thickness the first order reflection minimum red-shifts and consecutively overlaps the region where top, middle and bottom cell are most sensitive. By tuning the coating thickness it should therefore be possible to selectively enhance the current in top, middle or bottom cell.

GENPRO4 was used to simulate the triple junction cell with $MgF_2$ coating. Fig. 6a shows the simulated top, middle and bottom cell current density as a function of coating thickness. This reveals that the optimum $MgF_2$ coating

thicknesses for maximum currents from top, middle and bottom cell are 88 nm, 110 nm and 130 nm, respectively. Overall, the optimum coating thickness is 110 nm, as this increases the top, middle and bottom cell currents by 1.7%, 2.0% and 1.7%, respectively. When starting from a perfectly current matched device, as shown in Fig. 6a, the $MgF_2$ coating will therefore increase the device current by 1.7%. Note however that when starting from a slightly mismatched device, the highest device current may be achieved by targeting the cell that is limiting the current. For example when the device current is limited by the bottom cell (as for the initial configuration considered in Fig. 4b), a 130 nm coating would enhance the device current by 1.8% while a 110 nm coating would enhance this by only 1.7%.

Fig. 6a also shows a second set of maxima for coating thicknesses of more than 200 nm. These maxima are caused by the *second* order reflection minimum passing over the spectral regions where respectively top, middle and bottom cell are most sensitive. Interestingly, because the second order reflection minimum is much narrower, the current of the individual cells can be enhanced more selectively. For example, a 260 nm thick $MgF_2$ coating enhances the top cell current by 1.3%, without affecting the bottom cell current.

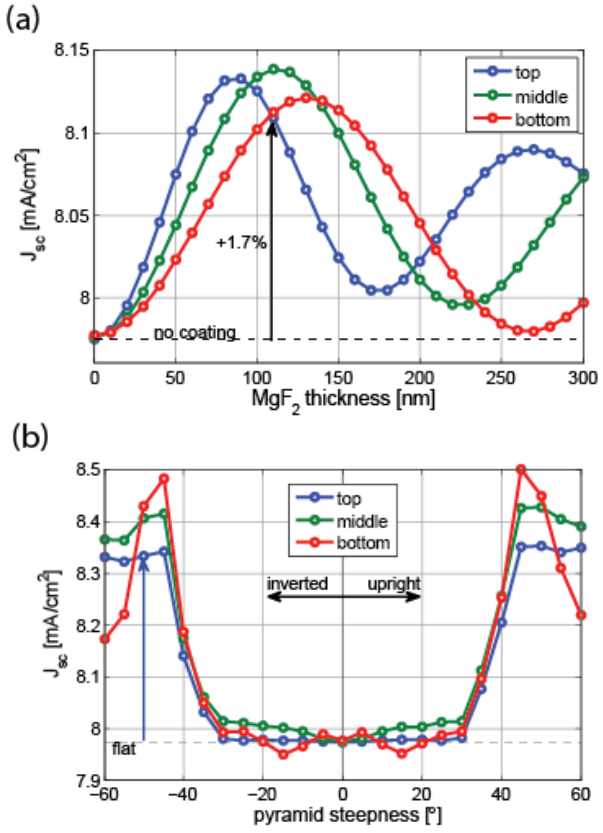


Fig. 6. Top, middle and bottom cell implied photocurrent density. a) As a function of $MgF_2$ coating thickness. b) As a function of texture foil pyramid steepness.

A second approach for reducing reflectance loss is to apply a transparent polymer at the air/glass interface that has a texture with a feature size in the micron to millimeter range [31]. Here we will consider a square base pyramid texture. Such a foil will reduce reflectance loss when any light reflected off one pyramid hits a neighboring pyramid and enters the material. To which extent this occurs depends on the steepness of the pyramid (i.e. the angle the pyramid face makes with the horizontal). As long as the pyramids are larger than the wavelength of the incident light, ray optics applies and the anti-reflective properties do not depend on the exact size of the pyramid. Unlike the $MgF_2$ coating, this anti-reflective foil will cause a *broadband* reflection reduction that affects the top, middle and bottom cell in the same way. However, refraction of light by the texture changes the propagation direction of light inside the device. The light will be scattered in somewhat different directions at each of the nano-textured interfaces. Because every layer has a different, wavelength dependent, refractive index it is difficult to predict the overall effect in advance. Some layers might absorb more light, leaving less light for other layers thereby potentially creating some current mismatch between top, middle and bottom cell.

GENPRO4 was used to investigate the effect of such a pyramid textured anti-reflective foil. For simplicity it was assumed that the foil has the same optical properties as glass. Note that ray optics is used for the pyramid texture while wave optics was used for the nano-textured interfaces. The fact that ray and wave optics can be combined in this way shows the flexibility of GENPRO4. The pyramid steepness was varied between -60° and 60°, where a negative and positive steepnesses signify inverted and upright pyramids, respectively. Fig. 6b shows the top, middle and bottom cell currents as a function of pyramid steepness. This shows that a shallow pyramid with a steepness less than 30° has little effect. This steepness is insufficient to induce a second bounce and reduce reflectance. However, increasing the pyramid steepness from 30° to 45° does reduce reflectance and enhances all cell currents by about 5%, both for inverted and upright pyramids. About 4% of this gain can be attributed to reduced reflection losses and the additional 1% is due to increased path length inside the absorber layers. No significant further increase is observed when pyramid steepness is increased beyond 45°. Small differences between the cells can be observed. Especially for a pyramid steepness of ±45°, where the bottom cell current exceeds the current of the top cell by 1.8%.

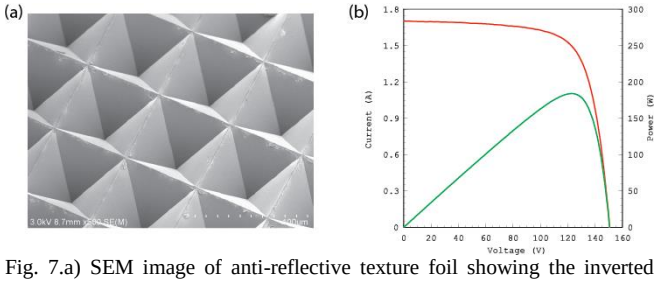


Fig. 7.a) SEM image of anti-reflective texture foil showing the inverted pyramid texture. b) IV-curve, measured independently by AIST in Japan, of the triple junction thin-film silicon PV module with an area of 1.42 m × 1.10 m with anti-reflective texture foil.

Based on these simulation results an anti-reflective texture foil was developed with inverted pyramids of 70 µm wide and with a steepness of -55°, as shown in Fig. 7a. This texture foil was then applied to a large area (1.42 m × 1.10 m) triple junction thin-film silicon PV module. As predicted by the model, the application of the foil increased the PV

module's current and power output. This resulted in a PV module power of 184 $W_p$, which corresponds to an initial conversion efficiency of 11.77%, as independently confirmed by measurement at the National Institute of Advanced Industrial Science and Technology (AIST) in Japan (shown in Fig. 7b). This is a very high efficiency for a thin-film silicon PV module of this size.

The results presented in this section have shown that both an $MgF_2$ coating and texture foil can enhance the device current of the triple junction thin-film silicon solar cell, but can also introduce a slight current mismatch. In order to arrive at the maximum device current, the cell currents need to be perfectly matched. Therefore the effects of $MgF_2$ coating or anti-reflective foil need to be taken into account when determining the optimum top, middle and bottom i-layer thickness. GENPRO4 was used to 'rematch' the currents by varying top and middle cell i-layer thicknesses. This was done for both the case of the device with either $MgF_2$ coating or with anti-reflective foil. The results are shown in Table 1 and the case with bare glass is given as a reference. Note that it was not needed to systematically go through all possible thickness combinations (as shown in Fig. 5a). Instead a simplex search algorithm was used to quickly find the top and middle cell thickness for perfect current matching.

TABLE I
TOP, MIDDLE AND BOTTOM CELL I-LAYER THICKNESS AND CORRESPONDING MATCHED CURRENT.

| | Top [nm] | Middle [nm] | Bottom [nm] | $J_{sc}$ [mA/cm$^2$] |
|---|---|---|---|---|
| Bare glass | 94.0 | 99.5 | 2300 | 7.98 |
| $MgF_2$ (110 nm) | 94.3 | 99.2 | 2300 | 8.12 |
| Foil (-55° pyramid) | 97.1 | 101.9 | 2300 | 8.45 |

## IV. CONCLUSIONS

GENPRO4 is a much improved version of our optical model for simulation of solar cells. It is based on the extended net-radiation method in which ray optics and wave optics are combined in a computationally efficient way. It can be used to gain insight in the optical losses of the solar cell and is especially suitable for quickly finding the absorber layer thicknesses needed for current matching in multi-junction solar cells.

The features of GENPRO4 are illustrated by simulation of a triple junction thin-film silicon solar cell. Very good agreement with EQE measurements is found. Simulations show that perfect current matching can be achieved by reducing the thicknesses of top and middle i-layer and thereby increasing the device current by 3.6%. A 110 nm thin $MgF_2$ anti-reflection coating on the front glass can increase the device current by an additional 1.7%. Alternatively, a foil with inverted or upright pyramid texture of at least 45° steepness can increase the device current up to 5%. Both the $MgF_2$ coating and the texture foil introduce a slight current mismatch which can be corrected by adjusting the i-layer thicknesses.

## ACKNOWLEDGEMENT

We would like to thank Olindo Isabella of Delft University of Technology for providing useful feedback on the manuscript and Klaus Jäger of Helmholtz-Zentrum Berlin for fruitful discussions.

## REFERENCES

[1] R.E.I. Schropp, M. Zeman, *Amorphous and microcrystalline silicon solar cells: Modeling, materials and device technology* (Springer,1998).

[2] M. Zeman, J. Krč, "Optical and electrical modeling of thin-film silicon solar cells," J. Mater. Res. **23**(4), 889–898 (2008).

[3] D.A. Clugston, P.A. Basore, "PC1D version 5: 32-bit solar cell modeling on personal computers," in *Proceedings of IEEE photovoltaic specialists conference* (IEEE,1997), pp. 207–210.

[4] J. Krč, F. Smole, M. Topič, "Analysis of light scattering in amorphous Si:H solar cells by a one-dimensional semi-coherent optical model," Prog. Photovolt. **11**, 15-26 (2003).

[5] M. Burgelman, P. Nollet, S. Degrave, "Modelling polycrystalline semiconductor solar cells," Thin Solid Films **361-362**, 527-532 (2000).

[6] K. Jäger, D.N.P. Linssen, O. Isabella, M. Zeman, "Ambiguities in optical simulations of nanotextured thin-film solar cells using the finite-element method," Opt. Express **23**(19), A1060-1071 (2015).

[7] P. Campbell, M. Green, "Light trapping properties of pyramidally textured surfaces," J. Appl. Phys. 62, 243 (1987).

[8] K.R. McIntosh, S.C. Baker-Finch, "OPAL2: Rapid optical simulations of silicon solar cells," i*n Proceedings of IEEE photovoltaic specialists conference* (IEEE,2012), pp. 265-271,

[9] O.S. Heavens, *Optical properties of thin films* (Butterworth,1955).

[10] R. Siegel, "Net radiation method for transmission through partially transparent plates," Sol. Energ. **15**(3), 273–276.

[11] R. Santbergen, A.H.M. Smets, M. Zeman, "Optical model for multilayer structures with coherent, partly coherent and incoherent layers," Opt. Express **21**(102), A262–A267 (2013).

[12] B.E. Pieters, J. Krč, M. Zeman, "Advanced Numerical Simulation Tool for Solar Cells – ASA5," in *Proceedings of IEEE Conference on Photovoltaic Energy Conversion* (IEEE,2006), pp. 1513–1516.

[13] M. Zeman, O. Isabella, S. Solntsev, K. Jäger, "Modeling of thin-film silicon solar cells," Sol. Energ. Mat. Sol. Cells **119**, 94-111 (2013).

[14] J. Krč, M. Topič, *Optical modeling and simulation of thin-film photovoltaic devices* (CRC Press,2013).

[15] B. Lipovšek, J. Krč, M. Topič, "Optical model for thin-film photovoltaic devices with large surface textures at the front side," Informacije MIDEM **41**(4), 264–271 (2011).

[16] M. Topič, M. Sever, B. Lipovšek, A. Čampa, J. Krč, "Approaches and challenges in optical modeling and simulation of thin-film solar cells," "Sol. Energ. Mat. Sol. Cells **135**, 57-66 (2015).

[17] R. Santbergen, R.J.C. van Zolingen, "The absorption factor of crystalline silicon PV cells: A numerical and experimental study," Sol. Energ. Mat. Sol. Cells **92**(4), 432–444 (2008).

[18] R. Santbergen, J.M. Goud, M. Zeman, J.A.M. van Roosmalen, R.J.C. van Zolingen, "The AM1.5 absorption factor or thin-film solar cells," Sol. Energ. Mat. Sol. Cells **94**(5), 715–723 (2010).

[19] Y. Li, Y. Chen, Z. Ouyang, A. Lennon, "Angular matrix framework for light trapping analysis of solar cells," Opt. Express 23(24), A1707–A1719 (2015).

[20] N. Tucher, J. Eisenlohr, H. Gebrewold, P. Kiefel, O. Hohn, H. Hauser, J.C. Goldschmidt, B. Blasi, "Optical simulation of photovoltaic modules with multiple textured interfaces using the matrix-based formalism OPTOS," Opt. Express **24**(14), A1083–A1093 (2016).

[21] B.T. Phong, "Illumination for computer generated pictures,"Comm. ACM **18**(6), 311-317 (1975).

[22] K. Jäger, M. Fischer, R.A.C.M.M. van Swaaij, M. Zeman, "A scattering model for nano-textured interfaces and its application in opto-electrical simulations of thin-film solar cells," J. Appl. Phys. **111**, 083108 (2012).

[23] K. Jäger, "On the scalar scattering theory for thin-film solar cells," PhD thesis, Delft University of Technology (2012). doi:10.4233/uuid:4220e3ee-bdcb-4a46-ade1-470d3c2ad6da

[24] D. Zhang, I.A. Digdaya, R. Santbergen, R.A.C.C.M. van Swaaij, P. Bronsveld, M. Zeman, J.A.M. van Roosmalen, A.W. Weeber, "Design and fabrication of SiOx/ITO double-layer anti-reflective coating for heterojunction silicon solar cells," Sol. Energ. Mat. Sol. Cells **117**, 132–138 (2013).

[25] F.T. Si, D.Y. Kim, R. Santbergen, H. Tan, R.A.C.M.M. van Swaaij, A.H.M. Smets, O. Isabella, M. Zeman, "Quadruple-junction thin-film

silicon-based solar cells with high open-circuit voltage," Appl. Phys. Lett. **105**, 063902 (2014).

[26] H.Tan, A. Furlan, W. Li, K. Arapov, R. Santbergen, M.M. Wienk, M. Zeman, A.H.M. Smets, R.A.J. Janssen, "Highly efficient hybrid polymer amorphous silicon multijunction solar cells with effective optical management," Adv. Mat. **28**(11), 2170-2177 (2016).

[27] Photovoltaic materials and devices laboratory, Delft University of technology, Software platform http://www.ewi.tudelft.nl/en/the-faculty/departments/electrical-sustainable-energy/photovoltaic-materials-and-devices/software-platform/

[28] R. Santbergen, "Manual for solar cell optical simulation software: GenPro4," http://www.ewi.tudelft.nl/fileadmin/Faculteit/EWI/DocumentenAfdelingen/Electrical_Sustainable_Energy/PVMD/GenPro4_manual.pdf

[29] R.J. Potton, "Reciprocity in optics," Rep. Prog. Phys. 67,717- 754 (2004).

[30] T. Sasaki, Y. Koi, K. Yamamoto, M. Yoshimi, M. Ichikawa, "Stacked photoelectric converter," Patent No.: US 7,550,665 B2, Jun. 23 2009.

[31] C. Ulbrich, A. Gerber, K. Hermans, A. Lambertz, U. Rau, "Analysis of short circuit current gains by an anti-reflective textured cover on silicon thin film solar cells," Prog. Photovolt. **21**(8), 1672–1681.